doi:10.36487/ACG_repo/2063_80

Explicit numerical modelling of dynamic reinforcement

Y Marulanda University of Chile, Chile

JA Vallejos University of Chile, Chile

Abstract

The widespread preference for the use of rockbolts to provide adequate rock stability in underground openings calls for a better understanding of the response of these reinforcement elements. Although it is widely accepted that fully-grouted rockbolts provide better stability in areas with high ground stress conditions, we know little about the response of these elements, especially under dynamic loading conditions. Numerical modelling of dynamic testing for reinforcement, using the FLAC3D code, was therefore conducted to study the behaviour of fully-grouted threadbar bolts under dynamic loading conditions. In order to obtain results that represent the real response of the reinforcement elements, an explicit model was calibrated to the laboratory behaviour of a series of fully-grouted threadbars, commonly used as reinforcement in underground excavations in Chile, tested under dynamic loading conditions using an impact test. Model calibration focused on matching the different constitutive responses of the main model components: grout, bolt and confinement. Modelling results are presented in terms of loading stages of the force displacement curve, including the initial elastic response, plastic behaviour and bolt energy absorption capacity. Finally, the study addresses the choice of input parameters required for a realistic simulation of the response of fully-grouted threadbar bolts.

1 Introduction

One of the main challenges of underground mining is to control the large displacements and high strain rates produced by seismic events. The use of yieldable reinforcement systems is the most common solution, hence the representation of their dynamic behaviour through laboratory-scale dynamic testing.

Studies of the behaviour of reinforcement and retainment elements under dynamic loads at institutions such as Canada's CANMET Mining and Mineral Sciences Laboratories (CANMET-MMSL) and the Western Australian School of Mines (WASM) have evolved from simply comparing loads to analysing the capacity of support system elements to absorb energy from impacts and deformation during the dynamic loading process. Through laboratory-scale testing representative of in situ conditions, these institutions have sought to quantify the elements' deformation and energy absorption, resulting in comparative parameters and an adaptable design under dynamic loads.

However, the high cost of laboratory-scale testing in terms of preparation time and validation means that only a limited number of such tests are performed. Numerical modelling is an alternative that can be used to explain the deformation and absorption process as well as to enhance the results of laboratory testing. Yi & Kaiser (1994a), Tannant et al. (1995), Ansell (1999; 2005), Thompson et al. (2004), St-Pierre (2007) and Marambio et al. (2018) have modelled the dynamic behaviour of reinforcement elements in laboratory-scale testing with a focus on load-displacement relationships. However, although the grout/rockbolt interface is known to be where reinforcement elements most commonly fail in situ, the role of grout has not been fully incorporated into these models.

In light of the need to represent the dynamic response of both the bolt and the grout, Marulanda & Vallejos (2019) used the results of triaxial tests to capture the essential components of grout failure under dynamic load conditions, that is, cohesion weakening and frictional strengthening (CWFS) and the mobilised dilation angle as a function of plastic strain. Following this procedure, a consistent parameter set for the strain-hardening/softening Mohr-Coulomb constitutive model was implemented in FLAC3D numerical modelling software.

The next step in the numerical modelling of reinforcement systems under dynamic load conditions is the integration of the response of each component - bolt, grout, confinement medium/element and accessories (nut and washer) - in a bid to achieve a real representation of laboratory testing results.

This article summarises the proposed methodology for the numeric modelling of grout response and describes the improvements made to the development of the numerical modelling of an explicit reinforcement element since the study of Marambio et al. (2018).

2 Dynamic numerical model

The numerical model of dynamic testing was developed by Marambio et al. (2018). It has three main components: the test facility structure, the rockbolt and the grout (Figure 1). This model simulates the impact test equipment developed by CANMET-MMSL. The facility transforms potential energy into kinetic energy by dropping a mass from a given height on to the lower end of a rockbolt that is embedded in a pipe with grout, causing deformation and possible failure and simulating the in situ conditions (Yi & Kaiser 1992; 1994b).

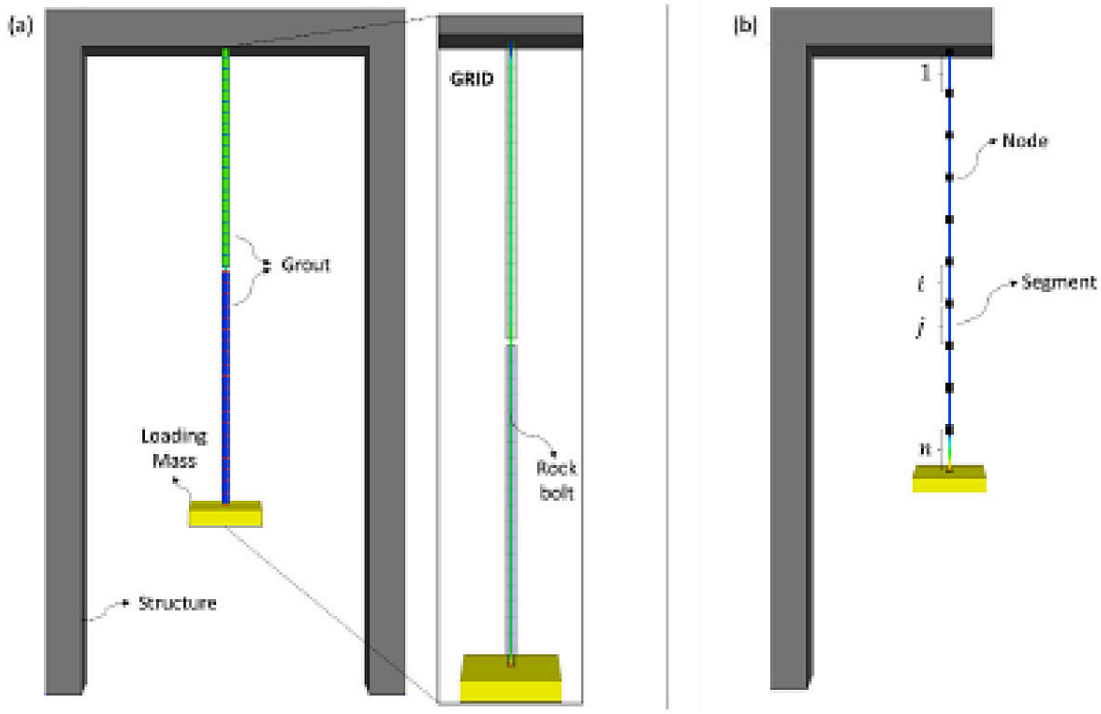

Figure 1 a) Model scheme in FLAC3D software; b) Reinforcement element represented by segments joined by nodes (Marambio et al. 2018)

Results obtained from the proposed numerical model showed good agreement with stress-strain curves from laboratory dynamic testing on threadbars (also known as rebars or gewibars), which are widely used as rock reinforcement in underground mining in Chile and the rest of the world. However, grout behaviour and interaction with the steel bar were not modelled.

3 Explicit numerical modelling

To arrive at a model that provides a more precise representation of the behaviour of the threadbar components under dynamic loading conditions, the mechanical behaviour of the grout was included in the principal FLAC3D model, applying mechanical properties to an explicit element that represents the grout.

The bolt is represented by a second explicit element. Rockbolt properties are well known and manufacturers' catalogues provide details of the properties of the material of their specific rock reinforcement elements. A fourth element, a steel tube as a confining element, was also modelled, represented by a DKT-CST

hybrid (DKT-CSTH) structural element (shell element) with the mechanical properties of steel. The new model configuration is shown in Figure 2.

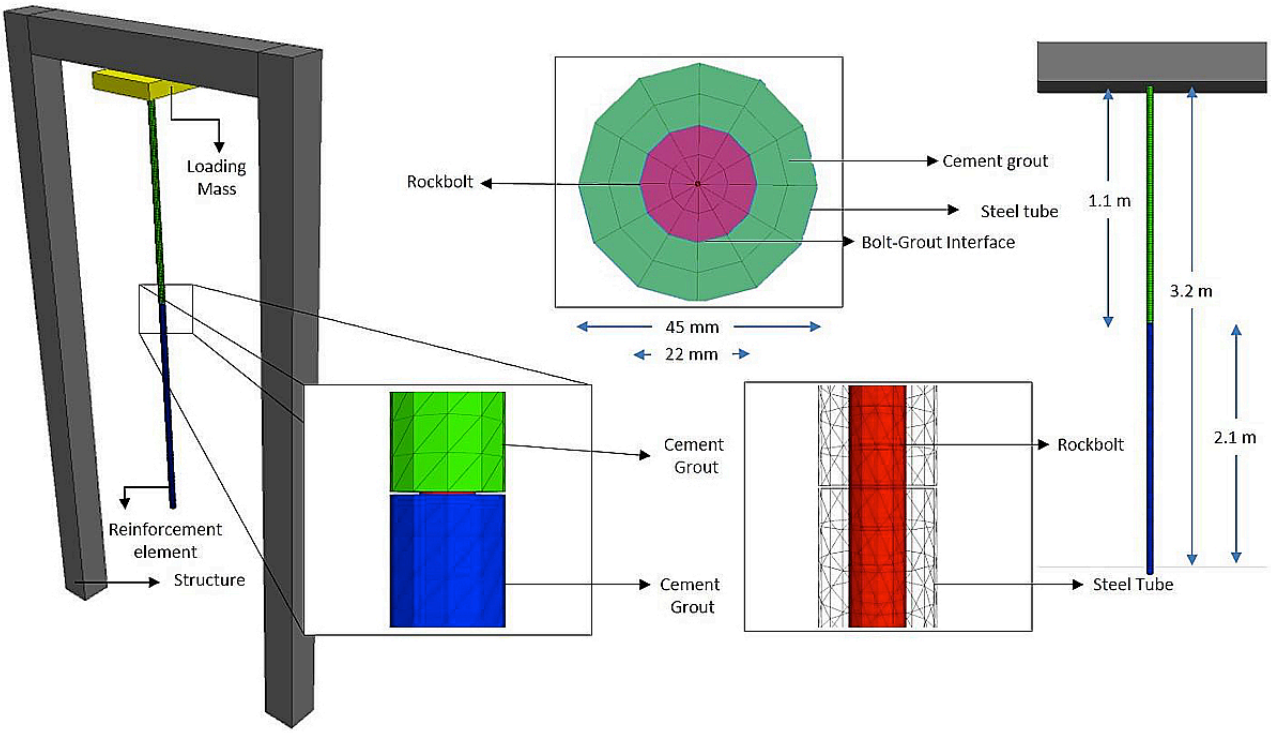

Figure 2 Model configuration comprising a confinement tube (shell), rockbolt (explicit element) and grout (explicit element)

3.1 Numerical model components

The proposed model uses the FLAC3D finite difference software (Itasca Consulting Group Inc. 2012), which is well known in the geomechanical and geotechnical industry. The system's components are described below.

3.1.1 Rockbolt

A rockbolt is represented in the model by an explicit element that responds to tension through an elastic-plastic constitutive model. The rockbolt is modelled using the Mohr-Coulomb criterion, controlled by bolt stiffness and yield limit. The mechanical properties correspond to the threadbar (Table 1).

However, steel is known to change its yield limit and ultimate strength under dynamic loading conditions. According to Malvar & Crawford (1998), these magnitudes can be estimated by the elastic properties of steel scaling through a dynamic increase factor as shown in Equation 1.

Equation 1 can be applied in function of a coefficient for the yield limit from Equation 2 or a coefficient for the limit and ultimate strength of steel from Equation 3. This proposal is, therefore, applied only to the response of the rockbolt (steel bar).

Table 1 Threadbar mechanical properties

Property	Value
Bar diameter	22 mm
Yield limit	167.258 KN
Tensile strength	440 MPa
Young's modulus *[E]*	210 GPa
Poisson's ratio	0.27
Density	7,850 Kg/m^3
Elongation	10 %

$$DIF = \left[\frac{\dot{\varepsilon}(t)}{10^{-4}}\right]^{\alpha_{fy},\alpha_{fu}} \quad (1)$$

$$\alpha_{fy} = 0.074 - 0.040\frac{\sigma_y}{414} \quad (2)$$

$$\alpha_{fu} = 0.019 - 0.009\frac{\sigma_y}{414} \quad (3)$$

Where:

DIF = Dynamic increase factor

$\dot{\varepsilon}$ = Strain rate

σ_y = Yield limit of steel in static condition in MPa

α_{fy}, α_{fu} = Coefficients for yield limit and ultimate strength of steel.

3.1.2 Grout

A group of explicit elements that envelop the threadbar represents the grout in which the rockbolt is inserted in the laboratory-scale dynamic tests.

3.1.2.1 Grout strength degradation model

The phenomenon of strain softening under compressive loads in cement grout (Figure 3) means that non-linear strength degradation is highly stress-dependent. As documented in triaxial tests conducted by Hyett et al. (1992) and Xie et al. (2008), the confining pressure and the grout's water-cement (w:c) ratio strongly affect the shape of the strength degradation as well as the value of the residual strength. Strength degradation decreases as confinement pressure increases. Finally, under high confinement pressure, the grout becomes almost ductile and no degradation occurs.

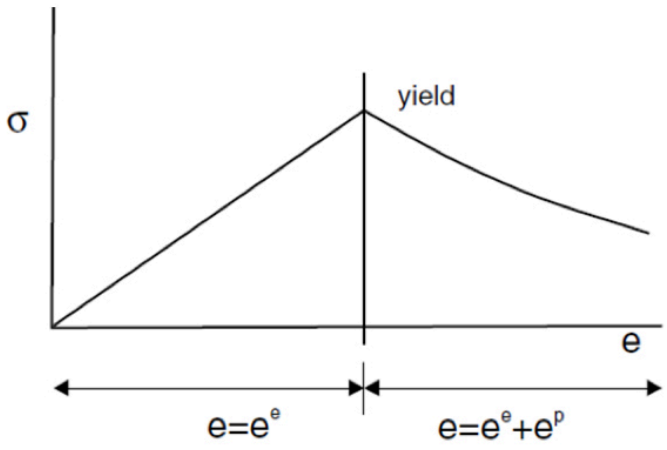

Figure 3 Strain softening/hardening model (Itasca Consulting Group 2012)

The variation of the degradation behaviour in relation to the confinement pressure can be defined using the cohesion-weakening-frictional-strengthening (CWFS) model proposed by Renani & Martin (2018). This proposal was enhanced to conserve the non-linear nature of damage and avoid sharp changes in the rate of cohesion degradation and friction mobilisation, as proposed by Hajiabdolmajid et al. (2002). Equations 4 and 5 were then used to describe the cohesion degradation and friction mobilisation of brittle material as smooth functions of plastic strain.

$$c = c_{ult} + (c_{ini} + c_{ult})\left[2 - \frac{2}{1+exp\,(-3.66\frac{\varepsilon^p}{\varepsilon_c^{p*}})}\right] \tag{4}$$

$$\varphi = \varphi_{ini} + (\varphi_{ult} - \varphi_{ini})\left[\frac{2}{1+expexp\,(-3.66\,\frac{\varepsilon^p}{\varepsilon_\varphi^{p*}})} - 1\right] \tag{5}$$

Where:

c_{ini}, c_{ult} = Initial and degraded values of cohesion

φ_{ini}, φ_{ult} = Initial and mobilised values of friction angle

ε_{c*}^p, $\varepsilon_{\varphi*}^p$ = Plastic strains at cohesion and friction angle are within 5% of their ultimate values, respectively.

Based on information from the literature (Hyett et al. 1992; Xi et al. 2008), the estimated parameters of the CWFS model for 0.4 and 0.44 w:c cement grout ratios are shown in Table 2, where E and ν are the modulus and Poisson's ratio of the cement grout, respectively. The variation in cohesion and friction and the corresponding stress-strain curves under triaxial compression tests are shown in Figure 4.

Table 2 Estimated parameters of the CWFS model for 0.4 and 0.44 w:c cement grout ratios. * Taken from Hyett et al. (1992)

w:c	σ_{ini} (MPa)	σ_{ult} (MPa)	E (Gpa)	ν	ε_{c*}^p	$\varepsilon_{\varphi*}^p$	φ_{ini} (°)
0.44	36.12	30.19	10	0.25	0.017	0.005	21.4
0.4	45.92	12.98			0.03	0.006	24

Table 2 Estimated parameters of the CWFS model for 0.4 and 0.44 w:c cement grout ratios (continued). * Taken from Hyett et al. (1992)

w:c	φ_{ult} (°)	C_{ini} (MPa)	C_{ult} (MPa)	Density (g/cm^3)*	Shear strength (Mpa)*
0.44	28.5	12	7.6	1.98	3.8
0.4	37	10	3	1.97	3.9

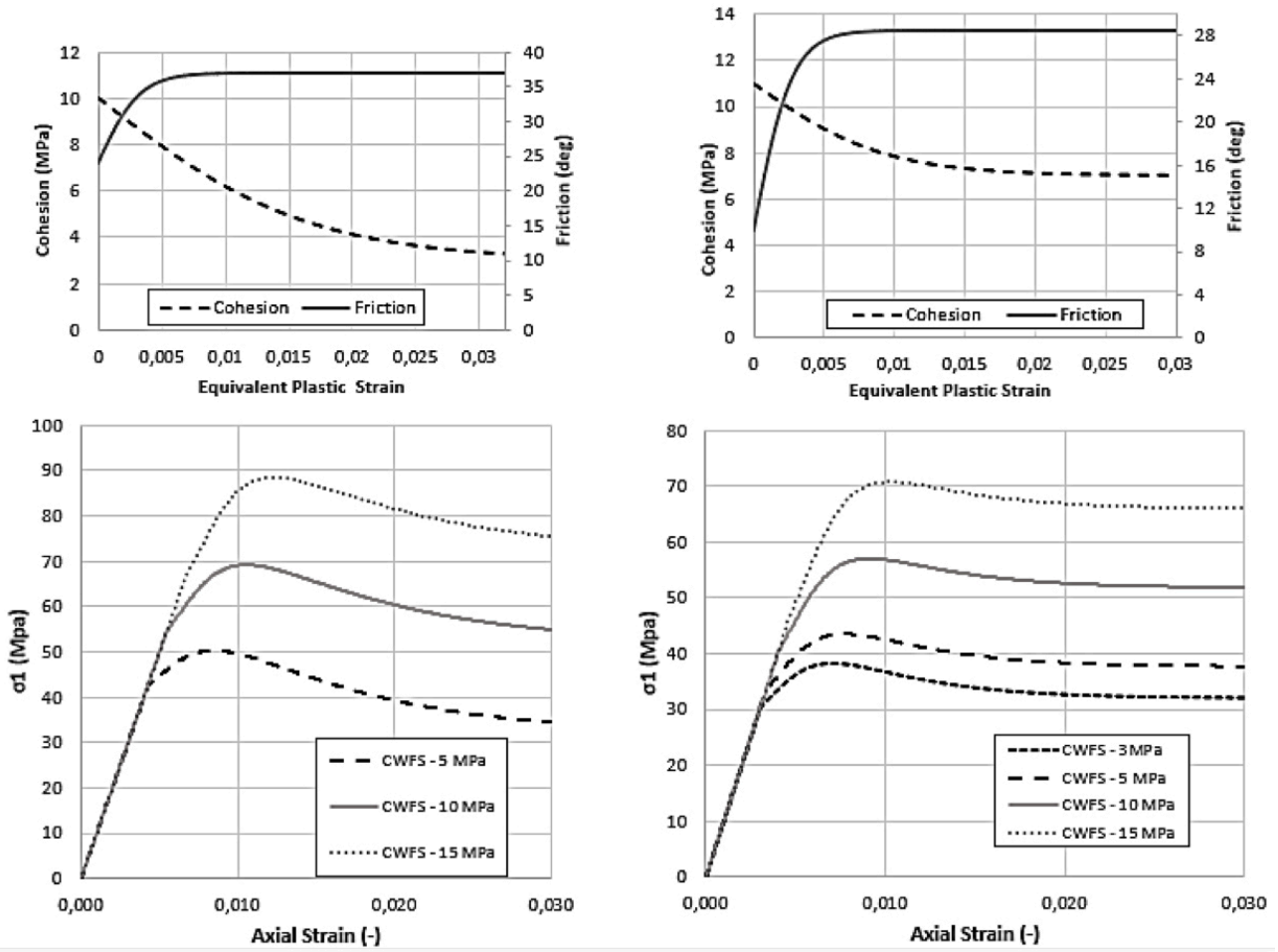

Figure 4 From top to bottom, cohesion loss and friction mobilisation and stress-strain curves under triaxial compression tests, respectively: (a) CWFS model response for 0.4 w:c cement grout ratio; (b) CWFS model response for 0.44 w:c cement grout ratio (Marulanda & Vallejos 2019)

The triaxial test data was analysed to deduce the cement grout's main geotechnical features. Peak and residual Hoek-Brown failure criteria were also fitted to the peak and residual strength values obtained from the testing.

3.1.2.2 Grout dilatancy model

A reasonable parameter for evaluating the plastic behaviour of the cement grout is the dilation angle ψ. As radial and axial stress-strain curves are available only for the 0.44 w:c cement grout ratio (Xie et al. 2008) for confinement pressures of 0, 3, 5 and 20 MPa, a point cloud for these curves of dilation angle was obtained as a function of the plastic parameter and confinement pressure, applying the proposal of Arzúa & Alejano (2013), (Figure 5). Alejano et al. (2005) proposed a dilatancy angle model that is divided into two parts, one referring to the peak dilation angle ψ_{peak} and the second related to dilation angle decay with plasticity as illustrated in Equations 6, 7 and 8.

$$\psi_{peak}(\sigma_3) = \frac{\phi_{peak}}{1+\sigma_c}\frac{\sigma_c}{\sigma_3+0.1} \tag{6}$$

$$K_\psi = 1 + (K_{\psi peak} - 1)^{e^{\frac{-\gamma^p}{\gamma^{p*}}}} \tag{7}$$

$$\gamma^{p,*} = \frac{\gamma^p}{lnln\left[(K_\psi - 1)/(K_{\psi,peak} - 1)\right]} \qquad \gamma^p = \left|\varepsilon_1^p - \varepsilon_3^p\right| \tag{8}$$

Where:

γ_{peak}, ϕ_{peak} = Peak dilation angle and peak friction angle, respectively

K_ψ, $K_{\psi peak}$ = Dilation angle decay with plasticity and dilation angle decay peak, respectively

γ^p, γ^{p^*} = Shear plastic strain and plasticity parameter constant, respectively

$\sigma_c, \sigma_3, \varepsilon_1^p, \varepsilon_3^p$ = Uniaxial compressive strength, confinement pressure, major and minor principal plastic strain, respectively.

Using this approach, the dilatancy angle for cement grout with a 0.4 w:c ratio was estimated for confinement pressures of 0, 5, 15 and 20 MPa. Three coefficients are, therefore, necessary to fit each of the curves shown in Figure 7. These coefficients are presented in Table 3.

Table 3 Fit coefficients for dilation angle-plastic parameter curves for cement grout with 0.4 w:c ratio

K_ψ				γ^p	γ^{p^*}
σ3 = 0 (MPa)	σ3 = 3 (MPa)	σ3 = 5 (MPa)	σ3 = 15 (MPa)	$(\mu strain)$	$(\mu strain)$
20	21	28	30	25	20

Laboratory test results for dilatancy were compared with the models proposed at different confinement pressures and plotted as shown in Figure 5. The model fits the laboratory data in terms of peak friction angle and the process of dilation decay.

Figure 5, therefore, reveals the expected behaviour with a dilation angle dependency as observed by Alejano et al. (2005). Thus, the dilation angle depends, first, on the confinement pressure (i.e. as confinement pressure increases, the dilation angle diminishes) and, second, on the plastic shear strain (i.e. as plastic shear strain develops, the dilation angle decays).

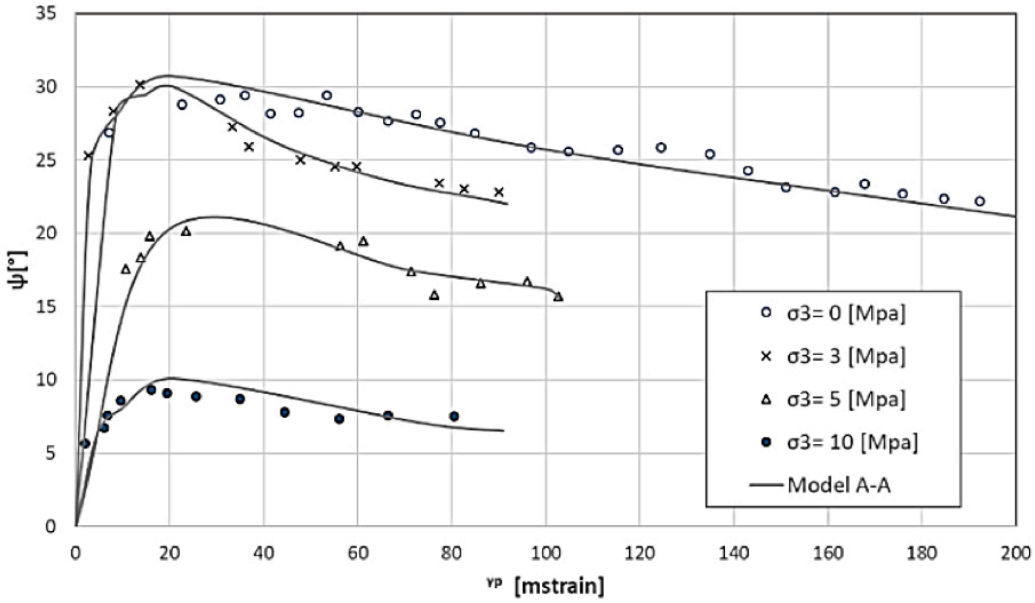

Figure 5 Dilatant behaviour for cement grout with 0.44 w:c ratio. Dilatancy from triaxial test compared with model proposed by Alejano & Alonso (2005)

Details of the determination of the fit coefficients for cohesion, friction and dilatancy and their application in numerical modelling for verification are presented in Marulanda & Vallejos (2019).

3.1.3 Confinement medium

A shell enveloping the grout represents the steel split pipe in which the grouted rockbolt is inserted in the laboratory-scale dynamic tests, applying confinement to the element tested. The split tube simulates the ground surrounding an excavation. During a seismic event, it constitutes both solid ground (steel pipe) and fractured plane (split) (Player et al. 2004).

In the numerical model, the shell responds to the tension through an elastic constitutive model controlled by Young's modulus E (F / L^2) and Poisson's ratio (ν) of steel. Its mechanical properties are shown in Table 4.

Table 4 Steel tube mechanical properties

Property	Value
Inner diameter	45 mm
Thickness	5 mm
Young's modulus [E]	210 GPa
Poisson's ratio	0.27
Density	7,850 Kg/m^3

3.2 Motion equations

To solve the numerical model, the dynamic system is divided into two secondary problems as illustrated in Figure 6. The first problem is described for the free fall of the mass used in the dynamic test until it impacts the plate (in the current test, a damping cushion) at a particular time (t_i). The second problem is in the interest of modelling and occurs after the moment of impact when the mass begins to move along with the rockbolt, stretching or sliding it until possible failure.

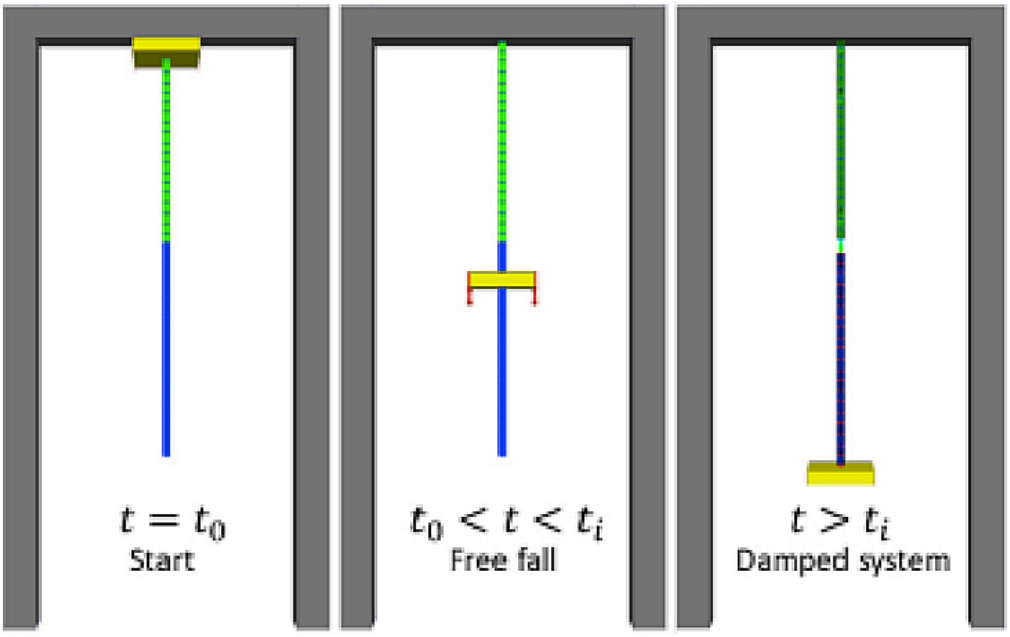

Figure 6 Scheme in FLAC3D software; from left to right, three temporal stages of the numerical model (Vallejos et al. 2019)

The system can, therefore, be represented by two differential equations, the first describing the motion of the rockbolt and the second the motion of the grout (Equations 9 and 10, respectively). A similar scheme can be found in St-Pierre (2007) in his development of a model for the cone bolt reinforcement element.

$$m\ddot{x}_b + c_b(\dot{x}_b - \dot{x}_g) + k_b(x_b - x_g) - F_{fk} + mg = 0 \quad (9)$$

$$m_g\dot{x}_g - c_b(\dot{x}_b - \dot{x}_g) - k_b(x_b - x_g) - c_g\dot{x}_g - k_g x_g + F_{fk} = 0 \quad (10)$$

Where:

m, m_g = Loading mass used in the dynamic test and grout mass, respectively

g = Gravity constant

k_b, k_g = Stiffness of rockbolt and grout, respectively

c_b, c_g = Viscous damping of rockbolt and grout, respectively

x_b, x_g = Displacement of rockbolt and grout, respectively

$\dot{x}_b, \dot{x}_g$ = Velocity of rockbolt and grout, respectively

$\ddot{x}_b, \ddot{x}_g$ = Acceleration of rockbolt and grout, respectively

F_{fk} = Friction force representing the contact between rockbolt and grout

The motion equations are solved using an iterative numerical method, explicit in time combined with the unbalanced force criteria from FLAC3D. The mass of the rockbolt (m_b) in Equation 9 and grout weight (m_g)) in Equation 10 are negligible in comparison to the loading mass of the dynamic test (m), which is around 200 times the mass of the rockbolt, and are, therefore, not taken into account in the motion equations. The stiffness of the rockbolt and the grout shown in Equations 7 and 8 are approximated by their equivalent stiffness for systems connected in series (Rao & Yap 2011).

The viscous damping of the rockbolt and the grout shown in Equations 9 and 10 are proportional to their respective masses, stiffness and a damping component, commonly known as classical Rayleigh damping (1877). The damping component mentioned above depends on the normal mode of vibration of the rockbolt (Den Hartog 1985), the grout (Nilsson 2009) and the strain rate.

Given the large difference between the physical and mechanical properties of the steel elements and the grout, an interface element was assigned at the rockbolt-grout interface. This is consistent with in situ experience in which most failures of reinforcement elements occur in the rockbolt–grout interface.

4 Modelling results

The mechanical behaviour of grout, established in Sections 3.1.2.1 and 3.1.2.2, and an interface representing possible slippage between the rockbolt and the grout were integrated into the principal $FLAC_3D$ model. The model defines the movement and impact of the loading mass as in the previous model and the difference in rockbolt behaviour lies mainly in the following aspects:

- The motion equations are invoked to derive new nodal velocities, displacements and forces in each zone representing the rockbolt and new strain rates are derived from the nodal velocities in order to apply the dynamic increase factor proposed by Malvar & Crawford (1998) in a constitutive elastic-perfectly plastic model. This is repeated at each step of calculation until the system reaches equilibrium.
- The confinement imposed by the encapsulating tube is represented by a DKT-CSTH structural element (shell element) (Itasca Consulting Group 2012) as its constitutive behaviour (elastic-perfectly plastic model).

Figure 7 presents the results obtained for the distribution of the maximum (S3) and minimum (S1) principal stresses along the grout (w:c 0.44). The failure of the element is located around the rockbolt de-bonded section, representing the laboratory results where, after the impact, the grout failed before the bolt.

When comparing the model grout zones response with images of the sample after the test (Player & Cordova 2009), a correlation between the failed zones is clear, indicating a good agreement of the model after the improvements made in Figure 8.

It should be noted that all the available mechanical parameters of the grout were considered and the model responds as expected according to experience in dynamic conditions. Nevertheless, research into the grout's behaviour under dynamic conditions is incipient and the results obtained from numerical modelling and the parameters used should be viewed and used with caution.

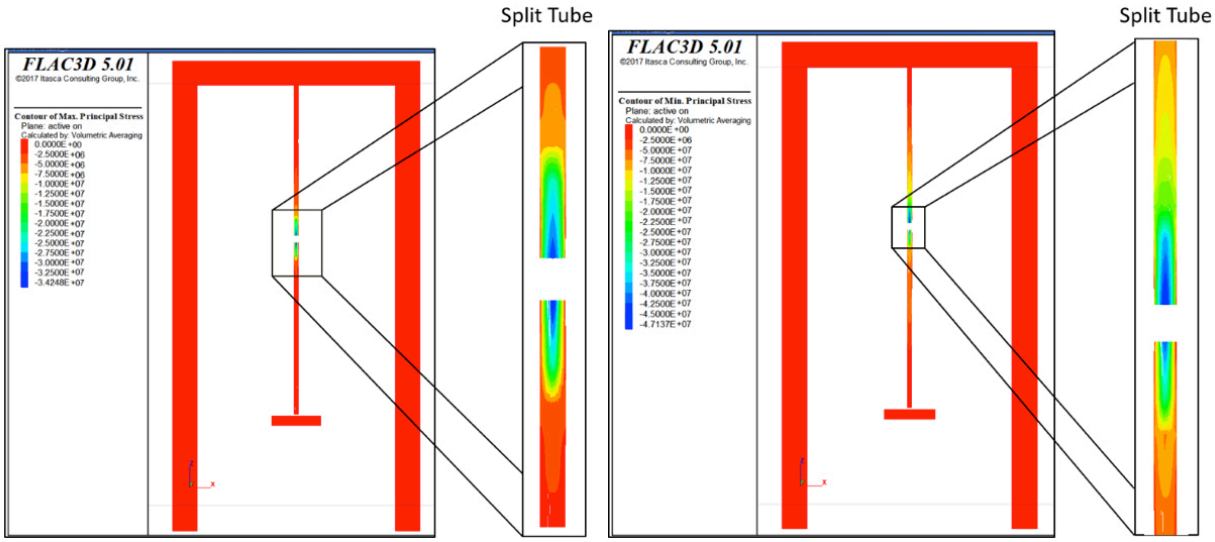

Figure 7 **S3 and S1 distribution along grout after impact obtained from numerical modelling**

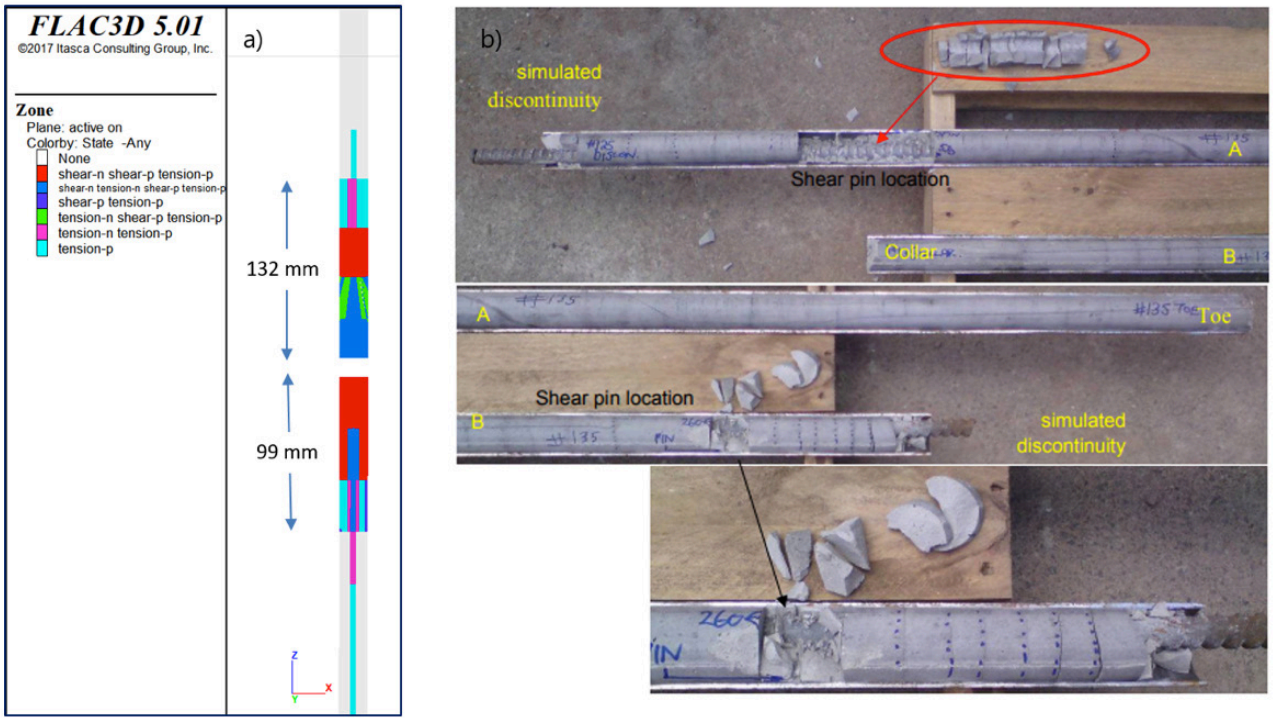

Figure 8 **a) Zone response in numerical modelling; b) Grout response after impact in WASM laboratory testing (Player & Cordova 2009)**

The test results from numerical modelling not only provide a visual approach. Figure 9 illustrates a numerical example of the load vs. displacement curves of the rockbolt in a final time stage of the model when equilibrium has been reached. A comparison between the model (simulated curve) and the WASM laboratory-scale dynamic test results (Player & Cordova 2009) is presented in Figure 9.

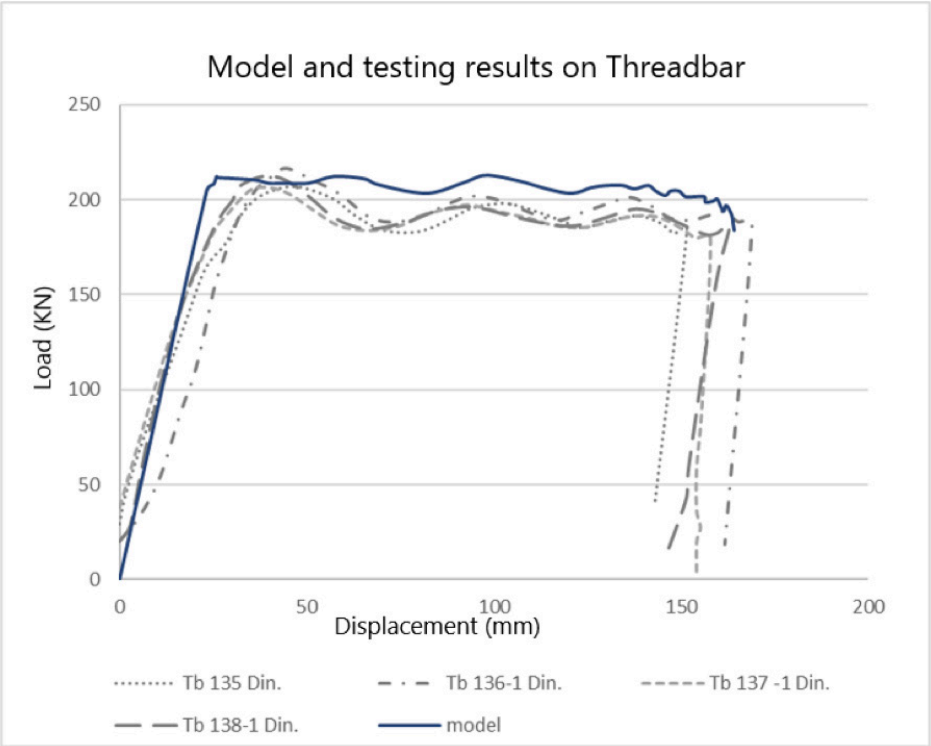

Figure 9 Load vs. displacement curves from numerical modelling and laboratory testing (Player & Cordova 2009)

The use of a complete set of mechanical parameters for grout and an explicit element to represent the steel tube in laboratory tests does not affect the final strength of the reinforcement element (Figure 9). These improvements influence mainly the system's initial stiffness when compared with results from Marambio et al. (2018).

5 Conclusions

The grout's role in overall system strength was determined. This component affects principally the system's initial stiffness as demonstrated by changes in the initial zone of the load vs. displacement curves when comparing with results obtained from numerical modelling carried out prior to the model presented in this paper. In previous models, the grout's mechanical response was not considered.

When analysing grout's independent response in modelled dynamic testing, it is seen to fail partially along the rockbolt in the expected zones due to the mechanical parameters assigned. This shows that the modified constitutive elements and parameters chosen are appropriate for describing the complete material behaviour of the grout used in cemented rockbolts, including the post-failure stage. Nevertheless, the proposed model's results should be verified through further results for the grout's dynamic response.

Numerical modelling is a useful tool for determining the response of a reinforcement element under dynamic loading conditions. At the current stage of the proposed model, the results are in good agreement with laboratory results. In the next step, the effect of reinforcement element geometry (rockbolt type) on the dynamic response of the system must be defined.

Acknowledgement

The authors gratefully acknowledge the financial support received from Basal Project FB-0809 Advanced Mining Technology Center (AMTC).

References

Alejano, LR, Alonso, E & Varas, F 2005, 'A model to estimate the dilatancy angle of rock masses', in Impact of Human Activity on the Geological Environment EUROCK 2005, Proceedings of the International Symposium EUROCK 2005, 18-20 May 2005, Brno, Czech Republic (p. 15). CRC Press.

Ansell, A 2005, 'Laboratory testing of a new type of energy absorbing rock bolt', Tunnelling and Underground Space Technology, vol. 20, no. 4, pp. 291-300.

Ansell, A 1999, 'Dynamically Loaded Rock Reinforcement' Institutionen för Byggkonstruktion, Stockholm.

Arzúa, J & Alejano, LR 2013, 'Dilation in granite during servo-controlled triaxial strength tests', International Journal of Rock Mechanics and Mining Sciences, vol. 61, pp. 43-56.

Den Hartog, JP 1985, Mechanical Vibrations, Dover Publications, New York.

Hajiabdolmajid, V, Kaiser, PK & Martin, CD 2002, 'Modelling brittle failure of rock', International Journal of Rock Mechanics and Mining Sciences, vol. 39, no. 6, pp. 731-741.

Hyett, AJ, Bawden, WF & Reichert, RD 1992, 'The effect of rock mass confinement on the bond strength of fully grouted cable bolts', International Journal of Rock Mechanics and Mining Sciences & Geomechanics Abstracts, vol. 29, no. 5, pp. 503-524.

Itasca Consulting Group Inc. 2012, 'FLAC3D', Itasca Consulting Group Inc. 2012, Minneapolis, https://www.itascacg.com/software/flac3d

Malvar, LJ & Crawford, JE 1998, 'Dynamic increase factors for steel reinforcing bars [C]', Proceedings of the 28th Department of Defense Explosives Safety Board Seminar, Department of Defense Explosives Safety Board, Alexandria.

Marambio, E, Vallejos, JA, Burgos, L, Gonzalez, Castro, L, Saure, JP & Urzua, J 2018, 'Numerical modelling of dynamic testing for rock reinforcement used in underground excavations', in Proceedings of the Fourth International Symposium on Block and Sublevel Caving, Vancouver, Canada, 15-17 October 2018, pp. 767-780.

Marulanda, Y, & Vallejos, J 2019, 'Modelling the response of reinforcement elements during dynamic loading', In 53rd US Rock Mechanics/Geomechanics Symposium, American Rock Mechanics Association.

Nilsson, C 2009, 'Modelling of Dynamically Loaded Shotcrete', Royal Institute of Technology.

Player, J & Cordova, M 2009, 'Dynamic Threadbar Test at WASM', Internal report for CODELCO - El Teniente Mine.

Player, JR, Villaescusa, E & Thompson, AG 2004, 'Dynamic testing of rock reinforcement using the momentum transfer concept', in E Villaescusa & Y Potvin (eds), Proceeding of the Fifth International Symposium on Ground Support, A.A. Balkema, Rotterdam, pp. 327-339.

Rao, SS & Yap, FF 2011, 'Mechanical Vibrations', Prentice Hall, Upper Saddle River.

Renani, HR & Martin, CD 2018, 'Modelling the progressive failure of hard rock pillars', Tunnelling and Underground Space Technology, no. 74, pp. 71-81.

St-Pierre, L 2007, 'Development and Validation of a Dynamic Model for a Cone Bolt Anchoring System', master's thesis, McGill University, Montreal.

Tannant, DD, Brummer RK & Yi, X 1995 'Rockbolt behaviour under dynamic loading: field tests and modelling', International Journal of Rock Mechanics and Mining Sciences & Geomechanics Abstracts, vol. 32, no. 6, pp. 537-550.

Thompson, AG, Player, JR & Villaescusa, E 2004, 'Simulation and analysis of dynamically loaded reinforcement systems', in E Villaescusa & Y Potvin (eds), Proceedings of the Fifth International Symposium on Ground Support, A.A. Balkema, Rotterdam, pp. 341-355.

Xie, SY, Shao, JF & Burlion, N 2008, 'Experimental study of mechanical behaviour of cement paste under compressive stress and chemical degradation', Cement and Concrete Research, vol. 38, no. 12, pp. 1416-1423.

Yi, X & Kaiser, PK 1994a, 'Elastic stress waves in rockbolts subject to impact loading', International Journal for Numerical and Analytical Methods in Geomechanics, vol. 18, no. 2, pp. 121-131.

Yi, X & Kaiser, PK 1994b, 'Impact testing for rockbolt design in rockburst conditions', vol. 31, no. 6, International Journal of Rock Mechanics and Mining Sciences & Geomechanics Abstracts, pp. 671-685.

Yi, X & Kaiser, PK 1992, 'Stress in dynamically loaded rockbolts with rubber and wood cushions', in PK Kaiser & DR McCreath (eds), Proceedings of the International Symposium on Rock Support: Rock Support in Mining and Underground Construction, AA Balkema, Rotterdam, pp. 683-691.